A Coupled Circuit and Field Analysis of a Stand-Alone Permanent-Magnet Synchronous Generator with Inset Rotor

T. F. Chan*, Lie-Tong Yan and L. L. Lai*****

Abstract - By using a coupled circuit, time-stepping, two-dimensional finite element method (2-D FEM), the performance of a stand-alone permanent-magnet synchronous generator (PMSG) with inset rotor can be computed without involving the classical two-axis model. The effects of interpolar air gap length and armature resistance on the load characteristics are investigated. It is shown that the interpolar flux density, and hence the amount of voltage compensation, is affected by magnetic saturation. Validity of the coupled circuit and field analysis is confirmed by experiments on a prototype generator. The machine exhibits an approximately level load characteristic when it is supplying an isolated unity-power-factor load.

Keywords: Finite element analysis, magnetic saturation, permanent-magnet synchronous generator (PMSG)

1. Introduction

PERMANENT-MAGNET synchronous generators (PMSGs) are increasingly used for stand-alone power systems. For such applications, the voltage regulation is of primary importance since the field excitation cannot be varied. It has been shown that, by using a PMSG with interior magnet rotor [1] or inset rotor [2], the voltage regulation can be significantly improved. Performance analysis of these machine configurations, however, is complicated by the unconventional rotor structure, complex magnetic saturation conditions, and changes in material properties.

This paper discusses the performance analysis of a three-phase PMSG with an inset rotor and supplying an isolated load. By using a time-stepping, two-dimensional (2-D) FEM, the steady-state performance of the PMSG can be directly computed without using the two-axis model and the concept of synchronous reactances. The validity of the analysis will be verified by experiments performed on a prototype machine.

2. Prototype Generator and Analysis

Fig. 1 shows the cross-section of a prototype four-pole PMSG with inset rotor[2]. The rotor magnet material is neodymium-iron-boron (NdFeB) whose recoil permeability is close to that of air. Each magnet is arch-shaped and is mounted on the surface of the rotor yoke. Soft-iron pole pieces are placed in the interpolar (quadrature-axis) regions. For high-speed operation, fibre glass binding tape or a metallic binding ring may be employed for better mechanical strength. The technical details of the prototype PMSG are given in Reference[2].

With reference to Fig. 1 and by choosing vector magnetic potential A as variables, the field equation and boundary conditions for the PMSG may be formulated as follows[3]-[5]:

$$\frac{\partial}{\partial x}\left(\frac{1}{\mu}\frac{\partial A}{\partial x}\right)+\frac{\partial}{\partial y}\left(\frac{1}{\mu}\frac{\partial A}{\partial y}\right)=-J \tag{1}$$

$$\left.\frac{1}{\mu_1}\frac{\partial A}{\partial n}\right|_{L^-}-\left.\frac{1}{\mu_2}\frac{\partial A}{\partial n}\right|_{L^+}=J_c \tag{2}$$

$$A|_{T1}=A|_{T2}=0 \tag{3}$$

where

J: externally impressed current density;
J_c: equivalent surface current density of PM material;
L^-: edge adjacent to L (see Fig. 1) and inside the PM material;
L^+: edge adjacent to L and outside the PM material;
N: normal direction;
$T1$: outer peripheral surface of stator core;
$T2$: inner peripheral surface of rotor core;
x, y: Cartesian coordinates;
μ: permeability;
μ_1: permeability of permanent-magnet material;
μ_2: permeability of air.

* Department of Electrical Engineering, The Hong Kong Polytechnic University, Hung Hom, Kowloon, Hong Kong, P.R. of China (eetfchan@polyu.edu.hk)
** Department of Electrical Engineering, Tsinghua University, Beijing, P.R. of China
*** The Energy Systems Group, School of Engineering, City University, Northampton Square, London EC1V 0HB, UK(L.L.Lai@city.ac.uk)
Received June 7, 2005 ; Accepted August 23, 2005

Depending upon the region being considered, (1) needs to be slightly modified. In sourceless regions, as in the case of the stator core and the rotor yoke, J should be equated to zero.

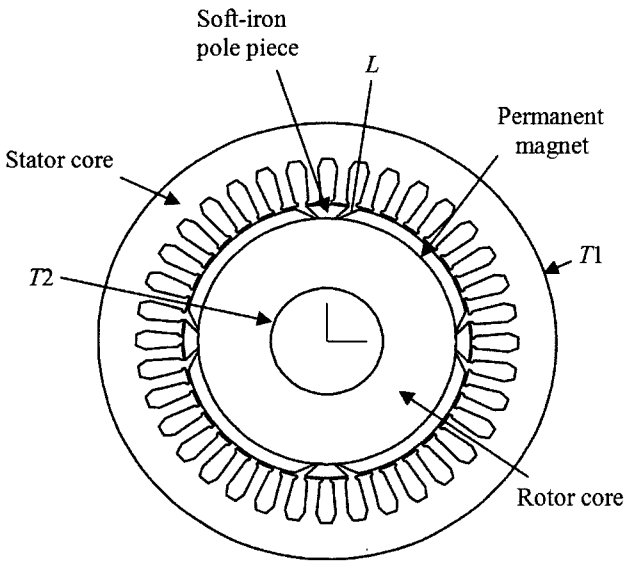

Fig. 1 Cross-section of prototype PMSG with inset rotor construction.

The energy functional $E(A)$ is given by

$$E(A)=\iint_{\Omega}\left(\int_{0}^{B}\frac{B}{\mu}.dB-A.J\right)dx.dy-\int_{L}J_C.A.dl' \tag{4}$$

where B is the flux density and dl' is an infinitesimal segment along edge L.

After discretization and functional minimization, the following matrix equation is obtained:

$$[K].[A]=[R] \tag{5}$$

where

$[K]$ coefficient (stiffness) matrix;

$[A]$ column matrix of nodal magnetic vector potentials;

$[R]$ right-hand side column matrix containing known terms.

The matrix equation (5) in the field domain has to be coupled to the external circuit. For a star-connected PMSG supplying an isolated load, the external circuit comprises the armature resistance R, the armature end-winding leakage reactance L_e, the load resistance R_L, and the load inductance L_L. Six circuit variables are introduced, namely the resultant generated phase e.m.f.s E_A, E_B, and E_C and the phase currents I_A, I_B and I_C.

Fig. 2 shows the mesh formation for the proposed analysis using time-stepping 2-D FEM. There are 2816 nodes and 5384 elements. The number of nodes with zero vector magnetic potential (i.e. nodes that fall on boundaries $T1$ and $T2$) total 248, hence the total number of field variables are 2816–248=2568. Since there are six additional circuit variables, the number of variables n' in the coupled circuit and field formulation are equal to 2568+6=2574.

Solution of the resulting simultaneous equations enable the nodal vector magnetic potentials, flux density, stator e.m.f.s, stator currents, and the terminal voltage to be determined. It should be noted that the synchronous reactances need not be evaluated throughout the solution procedure.

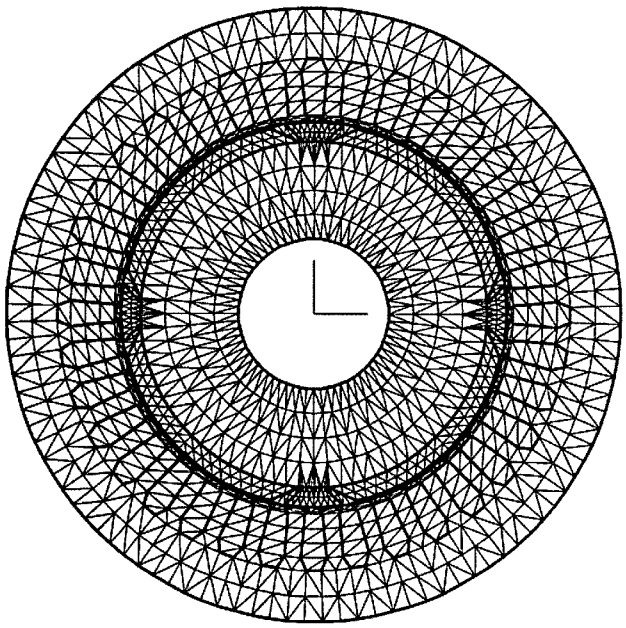

Fig. 2 Mesh formation for 2-D FEM analysis of PMSG with inset rotor.

In order to account for the effect of saturation, a magnetic nonlinearity subprogram needs to be included in the FEM solver. With the magnetic permeability μ of each element initialized to the appropriate value (for regions containing magnetic material, the unsaturated value of μ is used), the coefficient matrix $[K]$ is formed and modified according to the boundary conditions and the external circuit configureation. For each time step, the modified system of equations is solved and the flux densities in all the elements are evaluated from the nodal vector magnetic potentials. Using the magnetization curve of the magnetic material, the corresponding values of permeability μ (and hence the reluctivity υ) are updated. The computations are repeated until the iteration error $\Delta\varepsilon^2$ or the reluctivity error $\Delta\upsilon^2$ is within the specified limits, or the specified number of iterations has been reached. The iteration error $\Delta\varepsilon^2$ is defined as follows:

$$\Delta\varepsilon^2=\sum_{i=1}^{n'}[A_i'^{(k+1)}-A_i'^{(k)}]^2 \tag{6}$$

where

$A_i'^{(k+1)}$: value of ith variable of the modified column matrix $[A']$ in the $(k+1)$th iteration;

$A_i'^{(k)}$: value of ith variable of the modified column matrix $[A']$ in the kth iteration

The reluctivity error $\Delta\upsilon^2$ is defined as:

$$\Delta\upsilon^2 = \sum_{i=1}^{Ne}[\upsilon_{i,new}^{(k)} - \upsilon_i^{(k)}]^2 \tag{7}$$

where

$\upsilon_i^{(k)}$: value of reluctivity of the ith element at the beginning of the kth iteration;

$\upsilon_{i,new}^{(k)}$: value of reluctivity at the end of the kth iteration;

N_e : number of elements.

A relaxation factor is applied for updating the values of υ for the next iteration [5]:

$$\upsilon_i^{(k+1)} = \upsilon_i^{(k)} + W.(\upsilon_{i,new}^{(k)} - \upsilon_i^{(k)}) \tag{8}$$

where

$\upsilon_i^{(k+1)}$: value of reluctivity at the beginning of the $(k+1)$th iteration;

W: relaxation factor.

3. Computed Results

The algorithms presented in Section II were implemented in a FORTRAN program for analysis of the prototype PMSG. In the solver, each time step was equivalent to one mechanical degree, while a relaxation factor $W = 0.2$ was used in the magnetic nonlinearity subprogram. For each load impedance or operating point, the FEM computations were performed for 1440 steps (i.e. four complete revolutions of the rotor) to ensure convergence to the steady state. The solution procedure was therefore time-consuming due to the large number of variables involved and also the large number of steps required for the computations to converge. On a Pentium 4 personal computer with a clock speed of 1.6 GHz, the computation time for one operating point was approximately 7 h when magnetic saturation is neglected, and about 30 h when magnetic saturation is taken into consideration.

It is of interest to investigate the effect of interpolar air gap length g_{ip} on the load characteristic of the PMSG. Unity-power-factor loads were assumed for this comparison. The FEM computations were performed on the PMSG with g_{ip} varied. Fig. 3 shows the computed load characteristics, where g_{ip} = 0.35 mm refers to the prototype PMSG, while g_{ip} = 5.3 mm corresponds to a PMSG without interpolar pole pieces (i.e. a surface-magnet type PMSG). For the prototype generator, an almost level load characteristic is obtained, whereas in the surface-magnet PMSG, the load characteristic is quite linear but the phase voltage drops with increase of load.

Fig. 4 shows the load characteristics of the prototype PMSG when the armature resistance R is varied. It is apparent that the voltage compensation effect is improved when R decreases. For unity-power-factor loads, the PMSG exhibits a rising load characteristic when R = 0.062 Ω (one quarter that of the prototype generator in which R = 0.248 Ω). For 0.8 lagging-power- factor loads, reducing R also results in improvement in the output voltage, but a more drooping load characteristic is observed.

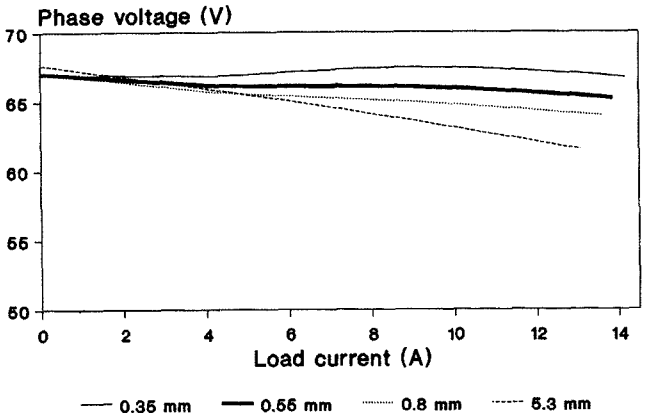

Fig. 3 Effect of interpolar air gap length g_{ip} on the computed load characteristic of PMSG when supplying a unity-power-factor load

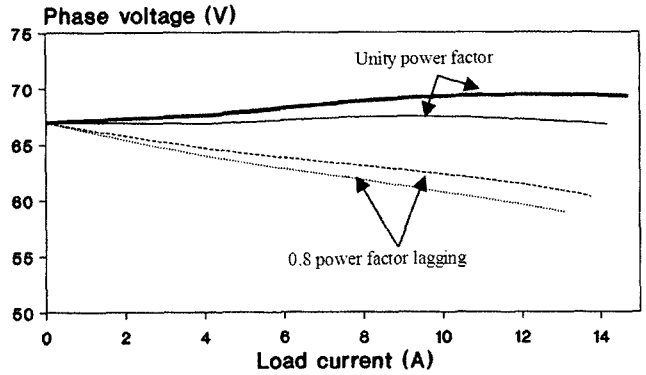

Fig. 4 Effect of armature resistance R on the load characteristics of the PMSG

The variations of the normal component of air gap flux density B_n with rotor position when the PMSG is supplying full-load armature current are shown in Fig. 5 (magnetic saturation being neglected) and Fig. 6 (magnetic saturation accounted for). It is observed that a high flux density exists in the interpolar regions, caused by the armature current and enhanced by the soft-iron pole pieces. Consequently the effecttive flux per pole is increased, resulting in an improvement in the voltage regulation. Without magnetic saturation,

B_n in the interpolar regions reaches 1.6 T (Fig. 5). When magnetic saturation is taken into consideration, the corresponding value of B_n is reduced to 0.9 T (Fig. 6). Magnetic saturation thus imposes a limit on the amount of voltage compensation that can be achieved.

Fig. 7 shows the computed line voltage and line current waveforms when the PMSG is supplying full-load current at unity-power-factor. It is seen that the harmonics have been suppressed to a large extent as a result of the distributed armature winding and the use of short-pitched coils.

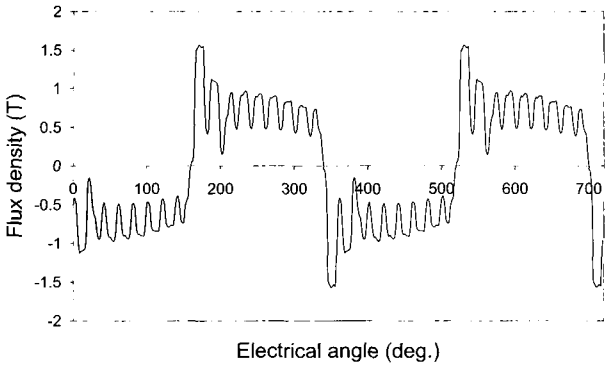

Fig. 5 Computed variation of B_n when the PMSG is supplying full-load armature current at unity-power-factor, magnetic saturation being neglected

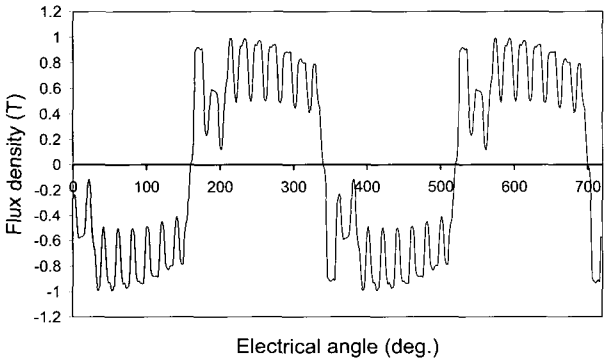

Fig. 6 Computed variation of B_n when the PMSG is supplying full-load armature current at unity-power-factor, magnetic saturation being accounted for

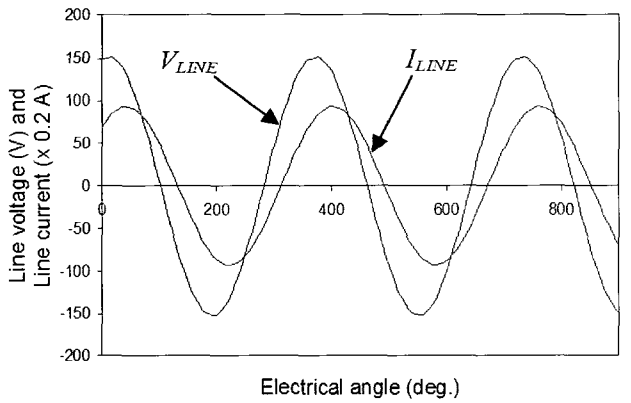

Fig. 7 Computed line-voltage (V_{LINE}) and line current (I_{LINE}) of the PMSG when supplying full-load current at unity-power-factor

4. Experimental Verification

A load test was performed on the prototype PMSG in order to validate the results computed using the coupled circuit, time-stepping 2-D FEM. The generator was driven at the nominal speed of 1500 r/min. A variable, balanced three-phase load was connected to the generator terminals and readings of load current and terminal voltage were recorded. Fig. 8 shows the computed and experimental load characteristics obtained. The computed characteristic is approximately level when the PMSG is supplying a unity-power-factor load and the full load voltage drop is only 6.4%. When the load power factor is 0.8 lagging, the voltage drop at full load increases to 12.7%. The voltage compensation capability of the PMSG with inset rotor is therefore better for unity-power-factor loads. Very good

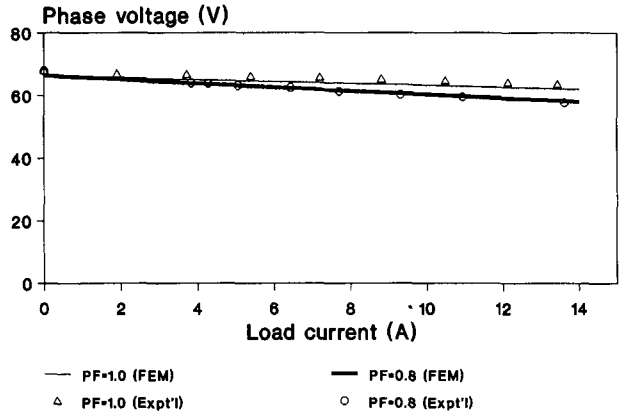

Fig. 8 Computed and experimental load characteristics of PMSG when supplying unity-power-factor and 0.8 lagging-power-factor loads at nominal speed

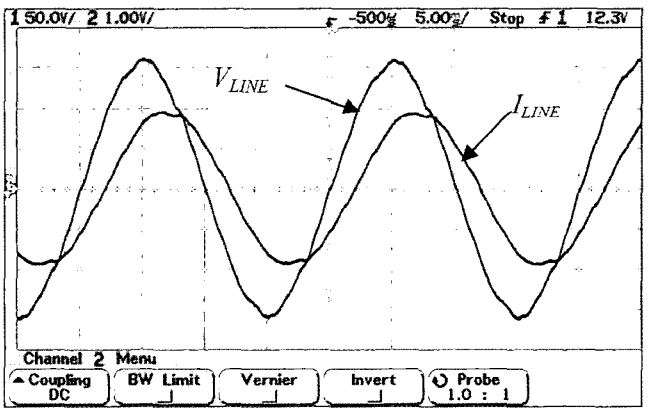

Fig. 9 Experimental line voltage (V_{LINE}) and line current (I_{LINE}) waveforms of PMSG when supplying full load current at unity power factor. (Voltage scale: 50 V/div; current scale: 10 A /div; time scale: 5 ms/div)

agreement between the computed and experimental characteristics has been obtained, confirming the accuracy of the coupled circuit and field method with magnetic saturation accounted for.

Fig. 9 shows the experimental line voltage and line current waveforms of the PMSG when supplying full load current at unity power factor. The experimental waveforms are similar to the computed waveforms shown in Fig. 7.

5. Conclusion

The performance analysis of a three-phase PMSG with inset rotor has been presented. A time-stepping, coupled circuit and field approach has been adopted and a two-dimensional finite element method is used for the field solution. It is demonstrated that the additional flux in the interpolar regions of the inset rotor results in automatic voltage compensation when the generator is supplying an isolated load. The good agreement between the computed and experimental results confirms the validity of the FEM model with magnetic saturation accounted for.

References

[1] B. J. Chalmers, "Performance of interior type permanent-magnet alternator," *IEE Proceedings – Electrical Power Applications*, vol. 141, no. 4, pp. 186-190, July 1994.

[2] T. F. Chan, Lie-Tong Yan, and L. L. Lai, "Performance of a three-phase a.c. generator with inset NdFeB permanent-magnet rotor," *IEEE Transactions on Energy Conversion*, vol. 19, no. 1, March 2004, pp. 88-94.

[3] S. L. Ho and H. L. Li, "Dynamic modeling of permanent magnet synchronous machines using direct-coupled time stepping finite element method," *IEEE International Electric Machines and Drives Conference (IEMDC '99)*, Seattle, Washington, USA, May 9-12, 1999, pp. 113-115.

[4] Pi-Zhang Chen, Lie-Tong Yan and Ruo-Ping Yao. *Theory and Computation of Electromagnetic Fields in Electrical Machines*. Beijing: Science Press, 1986.

[5] S. J. Salon. *Finite Element Analysis of Electric Machines*. Boston: Kluwer Academic Publishers, 1995.